Aerosol Chemical Speciation from MAIAC EPIC

Sujung Go[1,2], Myungje Choi[1,2], Alexei Lyapustin[2], Gregory L. Schuster[3]
1) UMBC GESTAR-II, 2) NASA GSFC, 3) NASA Langley

International Cooperative for Aerosol Predication (ICAP)
12th Technical Working Group Meeting, Oct. 18-21, 2022

Atmos. Chem. Phys., 22, 1395–1423, 2022
https://doi.org/10.5194/acp-22-1395-2022

Atmospheric Chemistry and Physics
Open Access
EGU

Research article

Inferring iron-oxide species content in atmospheric mineral dust from DSCOVR EPIC observations

Sujung Go[1,2], Alexei Lyapustin[2], Gregory L. Schuster[3], Myungje Choi[1,2], Paul Ginoux[4], Mian Chin[2], Olga Kalashnikova[5], Oleg Dubovik[6], Jhoon Kim[7], Arlindo da Silva[2], Brent Holben[2], and Jeffrey S. Reid[8]

[1]University of Maryland, Baltimore County, Baltimore, MD, USA
[2]NASA Goddard Space Flight Center, Greenbelt, MD, USA
[3]NASA Langley Research Center, Hampton, VA, USA
[4]Geophysical Fluid Dynamics Laboratory, Princeton, NJ, USA
[5]Jet Propulsion Laboratory, California Institute of Technology, Pasadena, CA, USA
[6]Univ. Lille, CNRS, UMR 8518 – LOA – Laboratoire d'Optique Atmosphérique, Lille, France
[7]Yonsei University, Seoul, Republic of Korea
[8]US Naval Research Laboratory, Monterey, CA, USA

Correspondence: Sujung Go (sujung.go@nasa.gov)

Received: 14 July 2021 – Discussion started: 27 August 2021
Revised: 19 November 2021 – Accepted: 3 December 2021 – Published: 27 January 2022

Brief introduction

- The dust direct radiative effect (DRE) at the top of the atmosphere is still controversial in both sign and magnitude. To resolve the issue, many previous studies primarily pointed out that current climate models are using globally invariant spectral complex refractive index (and therefore spectral SSA), which implicitly assumes the same dust mineralogical composition on a global scale.

- A few Earth system models, which is a coupled climate model, have adopted a regionally and temporally variable spectral refractive index of dust by parameterization with common soil mineralogy component (Scanza et al 2015; Perwidtz et al 2015a, b). The rationale for this is that dust aerosols are soil particles suspended in the atmosphere (Scanza et al., 2015).

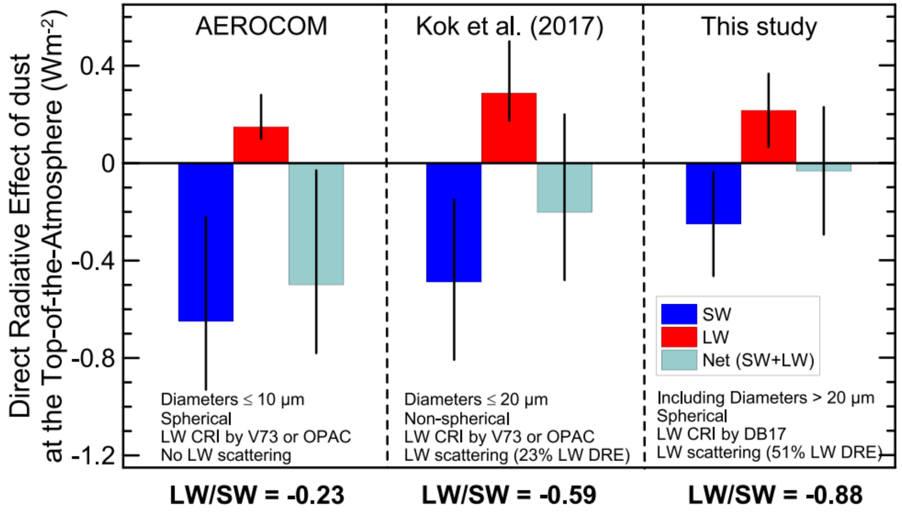

SW: 0.185-4.0 μm
LW: 3.33-1,000 μm
(Di Biagio et al., 2020)

- Li et al. (2021) recently quantified the importance of soil mineralogical content uncertainty on the dust DRE estimate. They concluded that the iron-oxide fraction in dust represents 97 % of the uncertainty in their estimated total dust DRE using CAM5 only and 85% across multiple climate models. It highlights the importance of distinguishing goethite from hematite for the shortwave dust DRE estimate. Otherwise, the model tends to underestimate dust warming at the TOA by ~56%, because the absorption magnitudes of hematite and goethite are up to an order of magnitude different at UV and Vis wavelengths.

Refractive index of soil mineralogy – Scanza et al. (2015)

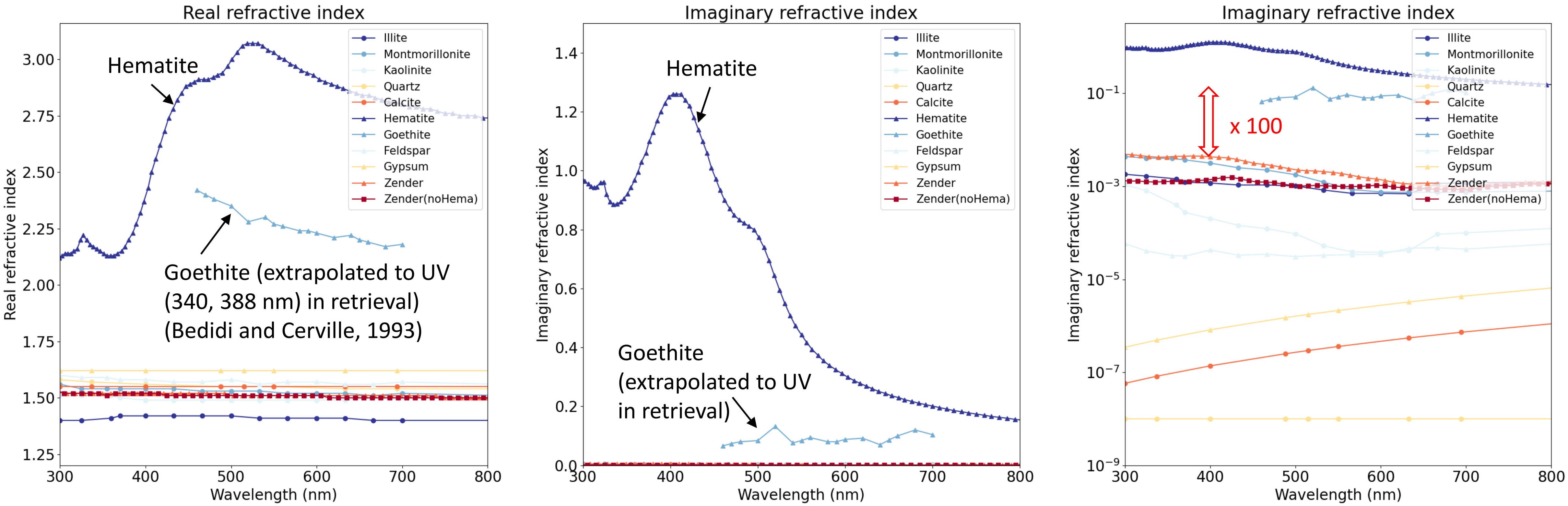

- Hematite (α-Fe_2O_3) and goethite (α-FeOOH), both in the Fe(Ⅲ) oxidation state, are the major iron oxides species in mineral dust (Torrent et al., 1983). They are major components controlling the absorption signal magnitude of pure dust toward SW radiation [e.g., Sokolik and Toon,1999; Moosmüller et al., 2012; Lafon et al., 2006; Formenti et al., 2014], as can be inferred from their complex refractive index imaginary part characteristics (Fig.1).

- We inferred hematite (α-Fe_2O_3) / goethite (α-FeOOH) content over main global dust source regions from MAIAC EPIC L2 products.

Distribution of iron oxide minerals in soil mineralogical map

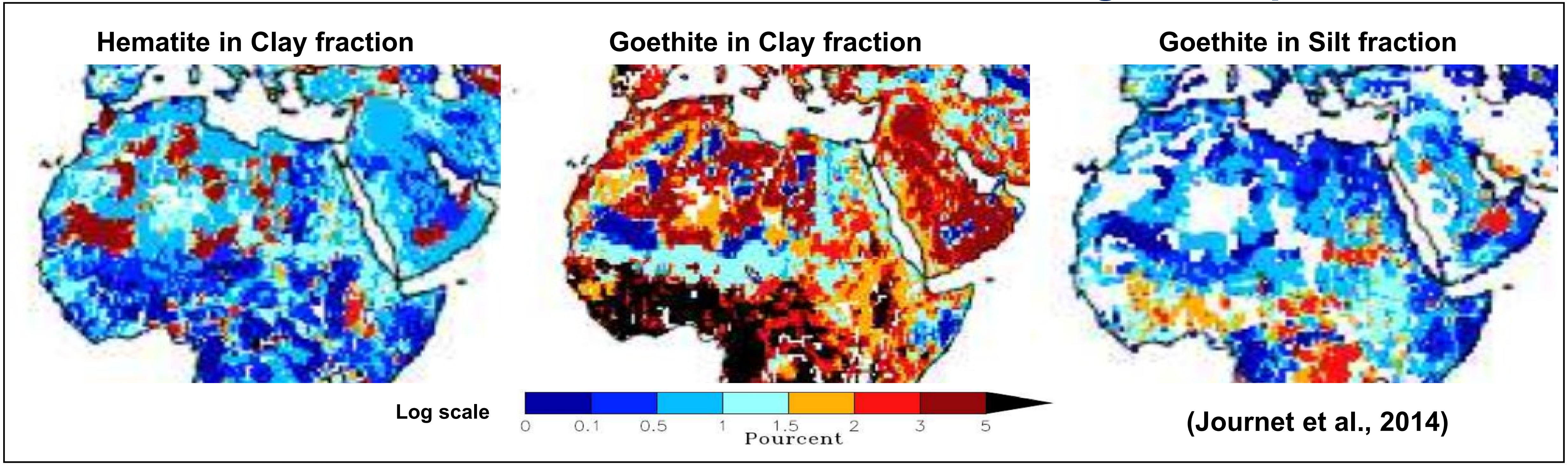

Journet, E., Balkanski, Y., & Harrison, S. P. (2014). A new data set of soil mineralogy for dust-cycle modeling. Atmospheric Chemistry and Physics, 14(8), 3801-3816.

- Specifically, for example in CAM5, dust aerosol mineralogy emission of two particle mode (accumulation mode Dp (μm): 0.1-1μm, coarse mode Dp (μm): 1-10μm) are transformed from soil mineralogy (clay-sized soil (Dp, 0-2μm), silt-sized soil (Dp, 2-50μm)) by brittle fragmen tation theory of dust emission (Kok, 2011) (Scanza et al., 2015; Liu et al., 2012).

- Then, dust aerosol refractive index is calculated from volume-weighted mixing rule of all mineral components including water and used a s input of RTM in CAM5. Here, mineral components are internally mixed within each particle mode, and externally mixed between differe nt particle mode (Liu et al., 2012, 2016).

Methodology - (Forward)

(1) With known refractive index ($\boldsymbol{n}, \boldsymbol{k}$) or complex dielectric function ($\boldsymbol{\varepsilon_r}$, $\boldsymbol{\varepsilon_i}$)

$$\varepsilon_1 = \varepsilon_{1,r} + i\varepsilon_{1,i} = (n_1^2 - k_1^2) + i(2n_1k_1)$$

$$\varepsilon_2 = \varepsilon_{2,r} + i\varepsilon_{2,i} = (n_2^2 - k_2^2) + i(2n_2k_2)$$

$$\varepsilon_h = \varepsilon_{h,r} + i\varepsilon_{h,i} = (n_h^2 - k_h^2) + i(2n_hk_h)$$

, where 1, 2, h indicates inclusion 1 (hematite), inclusion 2 (goethite), and host

(2) Maxwell Garnett effective medium approximation (f_1, f_2 : volume fraction of inclusions)

$$\varepsilon_{MG} = \varepsilon_h \left[1 + \frac{3\left(f_1\frac{\varepsilon_1-\varepsilon_h}{\varepsilon_1+2\varepsilon_h} + f_2\frac{\varepsilon_2-\varepsilon_h}{\varepsilon_2+2\varepsilon_h}\right)}{1 - f_1\frac{\varepsilon_1-\varepsilon_h}{\varepsilon_1+2\varepsilon_h} - f_2\frac{\varepsilon_2-\varepsilon_h}{\varepsilon_2+2\varepsilon_h}}\right] = \varepsilon_{MG,r} + i\varepsilon_{MG,i}$$

$$n_{mix} = \sqrt{\frac{\sqrt{{\varepsilon_{MG,r}}^2 + {\varepsilon_{MG,i}}^2} + \varepsilon_{MG,r}}{2}} \quad , k_{mix} = \sqrt{\frac{\sqrt{{\varepsilon_{MG,r}}^2 + {\varepsilon_{MG,i}}^2} - \varepsilon_{MG,r}}{2}}$$

$$m_{mix}(\lambda_j) = F(f_1, f_2, m_1(\lambda_j), m_2(\lambda_j), n_{host}(\lambda_j))$$

$$= n_{mix}(\lambda_j) + ik_{mix}(\lambda_j)$$

Illustration of Maxwell Garnett effective medium approximation (**pure dust**)
(Bohren and Huffman, 1987; Schuster et al., 2016)

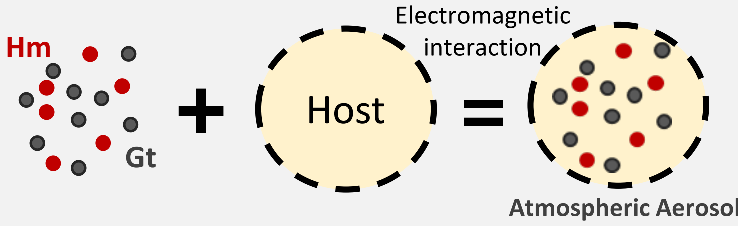

2 inclusions | Homogeneous matrix | Randomly inhomogeneous mixture

- **Assumption:** major absorption caused by hematite and goethite (not host)
- n_h = 1.52 (fixed), k_h = 0.0
- λ_j : 340, 388, 443, 680 nm
- **Fitting k_{epic} part only,** because MAIAC EPIC does not retrieve real part (n_{epic})

- (Inversion)

$$\chi^2 = \sum_{j=1}^{4}\left[\frac{(k_{epic}(\lambda_j) - k_{mix}(\lambda_j))^2}{k_{epic}(\lambda_j)}\right] \rightarrow min$$

MAIAC EPIC refractive index ($k_{epic}(\lambda_j) = k_{680}\,(\lambda_j/\lambda_{680})^{-b}$)
Updated iteratively

From EPIC AOD to composition mass concentration

- Step 1: calculate total (fine + coarse) volume concentration of dust (440 nm)
  - $\tau^a = \tau_f^a + \tau_c^a = C_{Vf}h_f + C_{Vc}h_c \approx C_{Vc}h_c$ ($\because C_{Vf} \ll C_{Vc}$ for AOD>0.6)
  - With $h_c = 1.2526$, $C_V \approx C_{Vc} = \frac{\tau^a}{1.2526} = 0.7983 * \tau^a$
  - C_V: volume concentration (μm³/μm²)
  - h_c: AOD per unit volume concentration

Volume concentration (μm³/μm²):

$$C_V = \int_{r_{\min}}^{r_{\max}} \frac{dV(r)}{d\ln r}\, d\ln r.$$

- Step 2: separate Hematite/Goethite volume concentration (C_V) using retrieved volume fraction (f) results
  - $C_{V,hematite} = C_V * f_{hematite}$
  - $C_{V,goethite} = C_V * f_{goethite}$
  - $C_{V,host} = C_V * f_{host} = C_V * (1 - f_{hematite} - f_{goethite})$

- Step 3: Then, calculate Hematite/Goethite mass concentration (C_M)
  - $C_{M,Hematite} = C_{V,Hematite} * \rho_{Hematite}$ ($\rho_{Hematite}$= mass concentration per unit volume (or density) = 5260 kg/m³)
  - $C_{M,Goethite} = C_{V,Goethite} * \rho_{Goethite}$ ($\rho_{Goethite}$= 3800 kg/m³)
  - $C_{M,Host} = C_{V,Host} * \rho_{Host}$ ($\rho_{Host} = \rho_{Zender}$ *= 2500 kg/m³)

    * Zender (Mahowald et. al., 2006) assuming Maxwell–Garnett mixing of 47.6 % quartz, 25 % illite, 25 % montmorillonite, 2 % calcite and 0.4 % hematite by volume with density equal to 2500 kg/m³ and hygroscopicity prescribed at 0.14 (Scanza et al., 2015).

    * Density of free iron is roughly twice that of other minerals (Schuster et al., 2016; Formenti et al., 2014).

  - ex) τ^a=0.75, $f_{hematite}$= 0.005

$$C_{M,Hematite} = \frac{\tau^a}{1.2526} * f_{hematite} * \rho_{Hematite} = \frac{0.75}{1.2526} * 0.005 * 5260 = 15.74 \text{ [mg/m}^2\text{]}$$

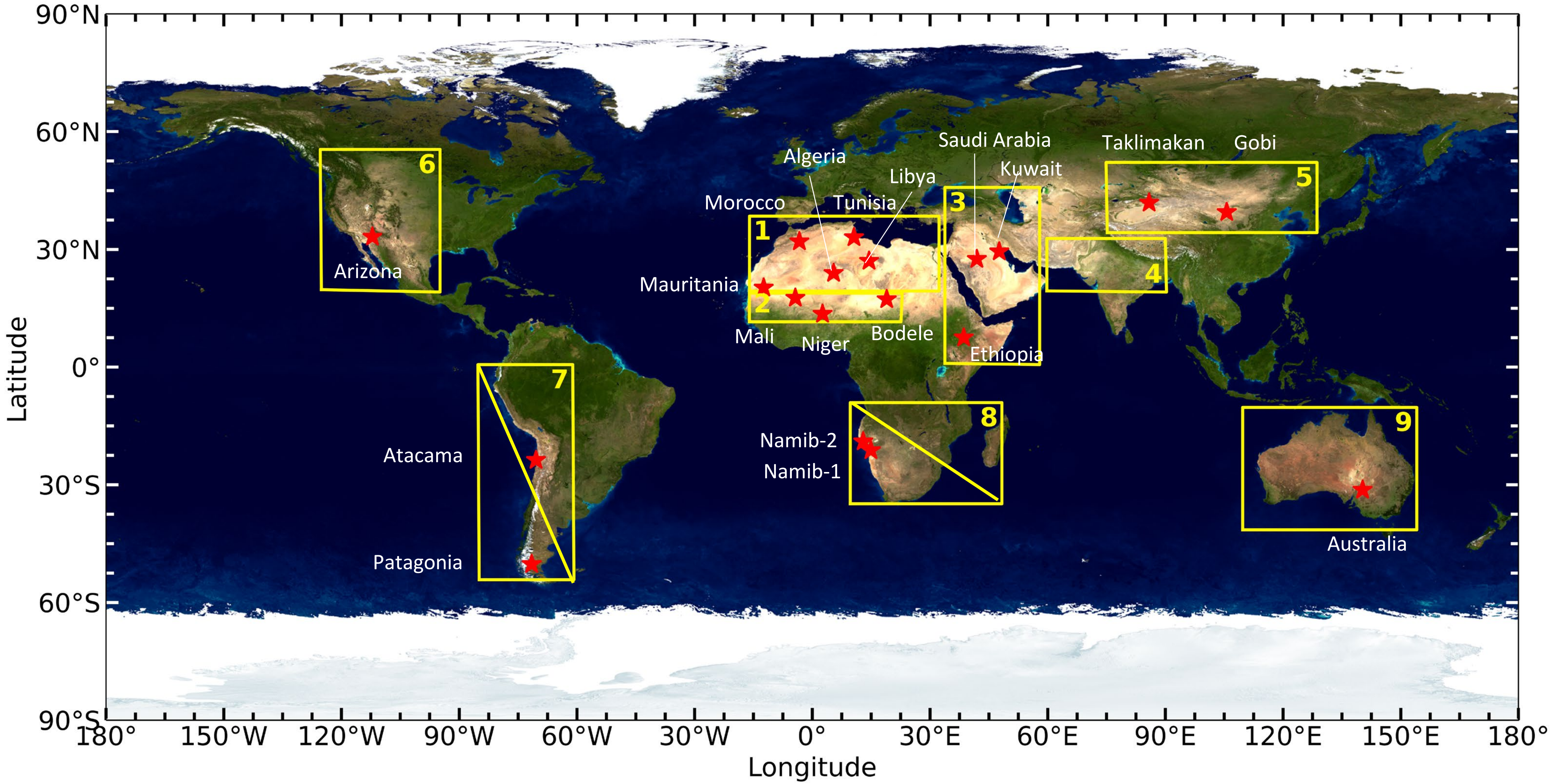

- Yellow rectangular - 9 different global main dust source regions (Ginoux et al., 2012; Di Biagio et al., 2017) ((1) northern Africa, (2) the Sahel, (3) eastern Africa and Middle East, (4) central Asia, (5) eastern Asia, (6) North America, (7) South America, (8) southern Africa, and (9) Australia)) – (7), (8) MAIAC EPIC do not provide dust

- Red star – Soil samples collected by Di Biagio et al. (2019).

- Di Biagio et al. (2019) sampled the 19 sites of source soil and investigated their properties including iron oxides contents, spectral complex refractive indices and spectral SSA.

Dust episodes - Sahara / Sahel

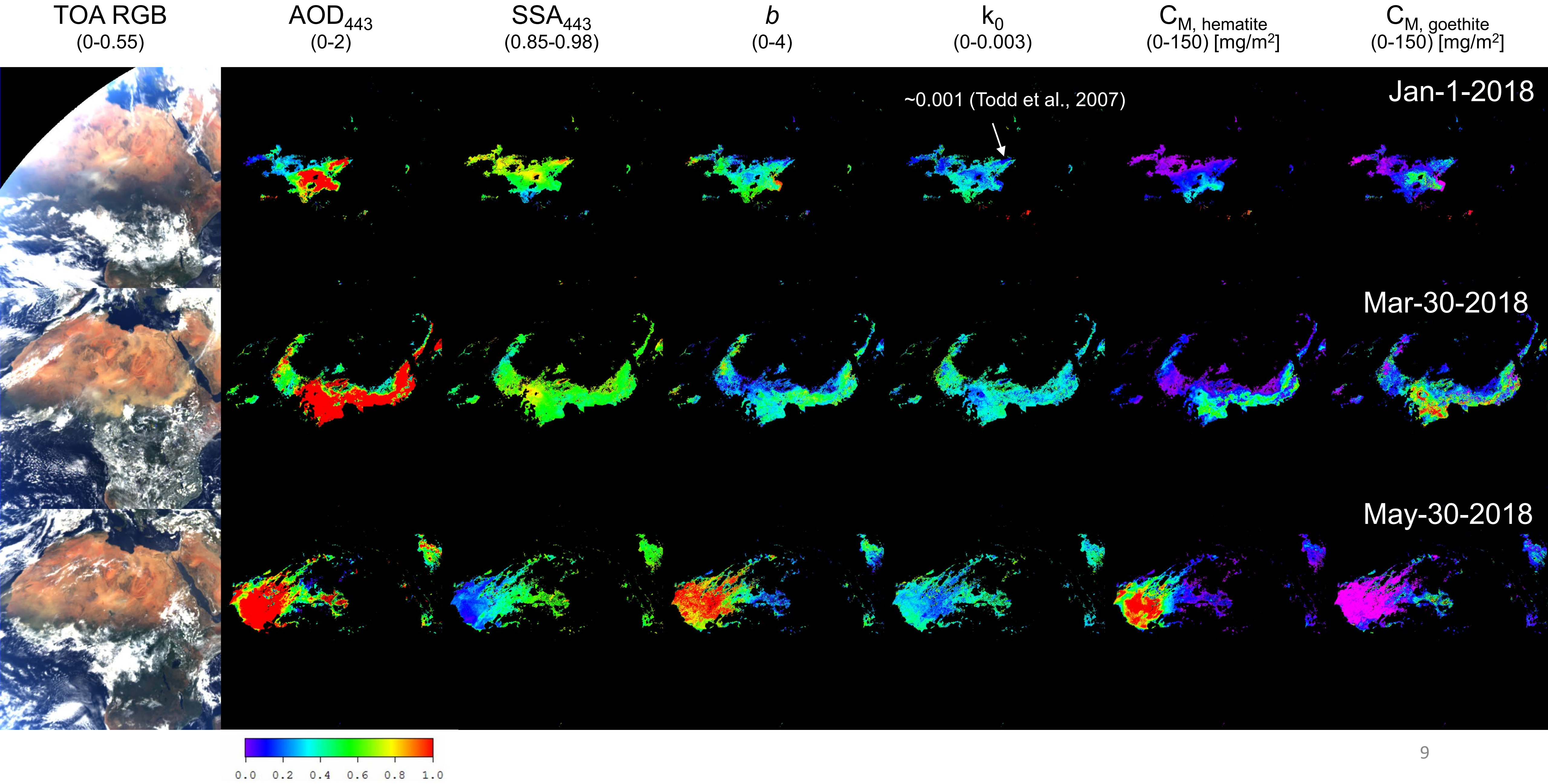

Dust episodes

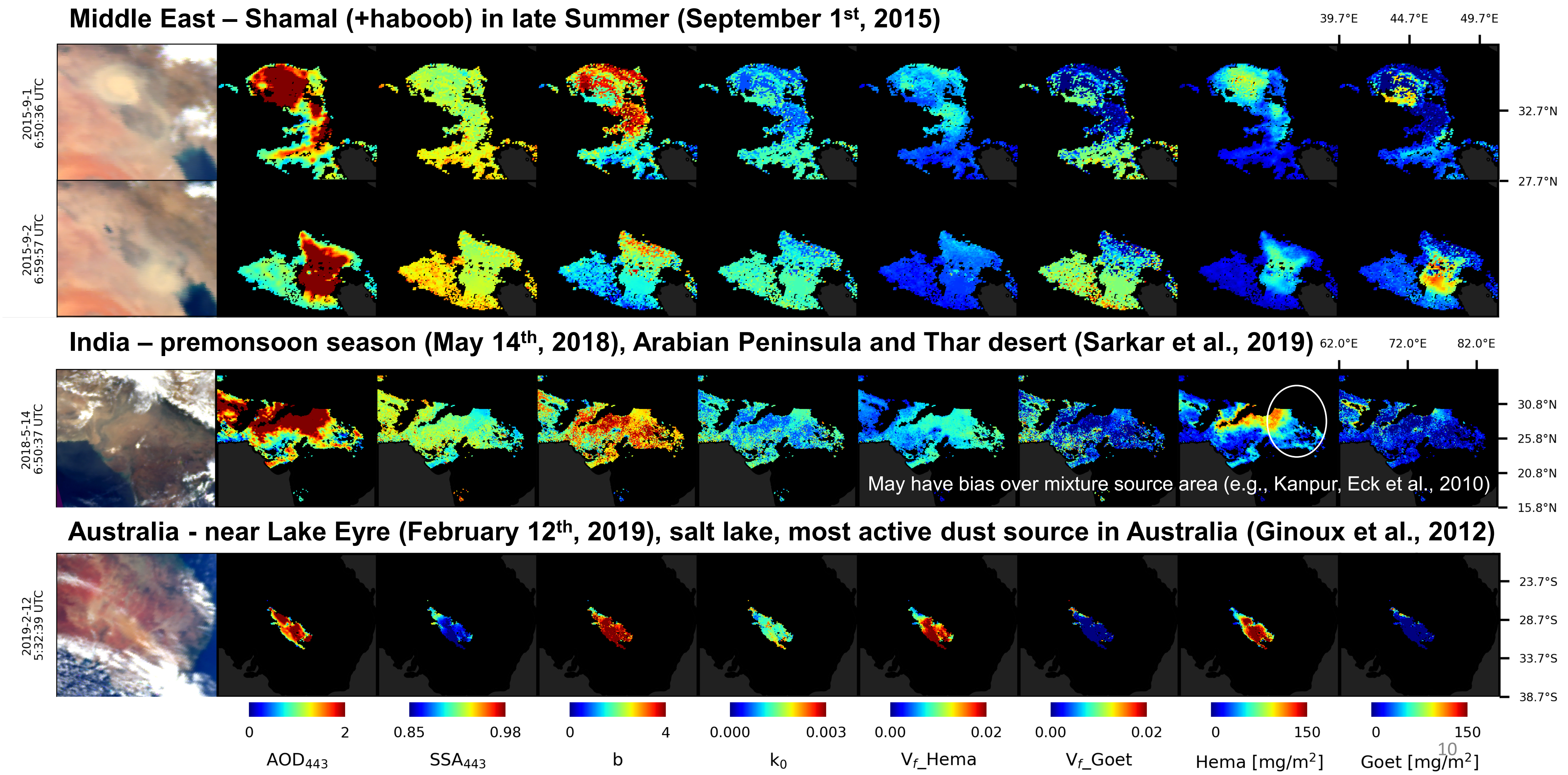

Bar plot for each cases

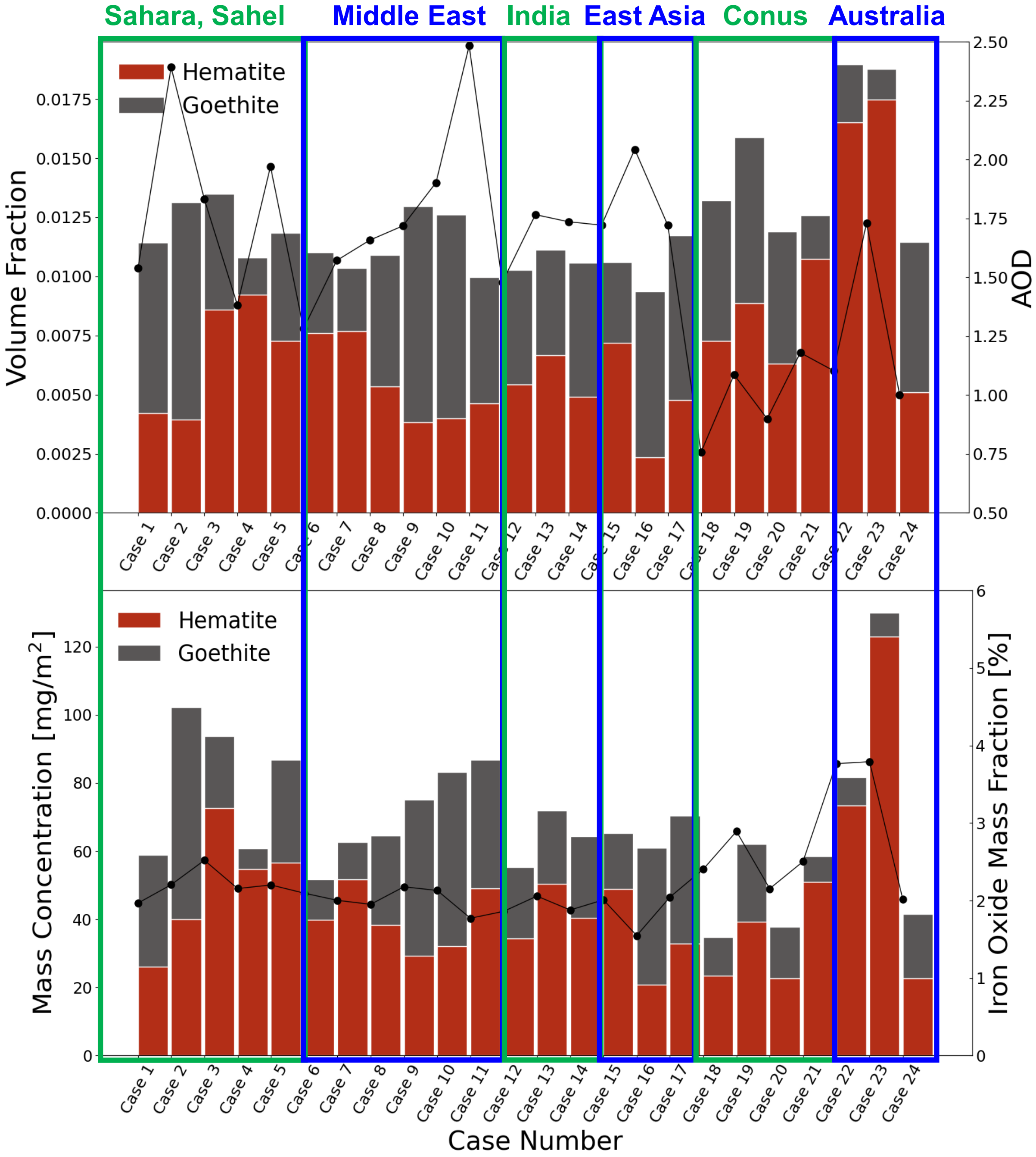

- **Mean** of each case studies (1 case/1 scene)
- **Mass Concentration**:
  Australia, Africa >> Middle East > India, EA > Conus
  → A few cases, therefore, cannot generalize here
- **(Australia)** low mean AOD, high volume fraction
  → high mass concentration
- **(Africa)** high AOD, low volume fraction (than Australia)
  → high mass concentration
- Iron oxide mass fraction (2~4 wt%) to the total dust

Comparison with Di Biagio et al. (2019)

Retrieval from EPIC

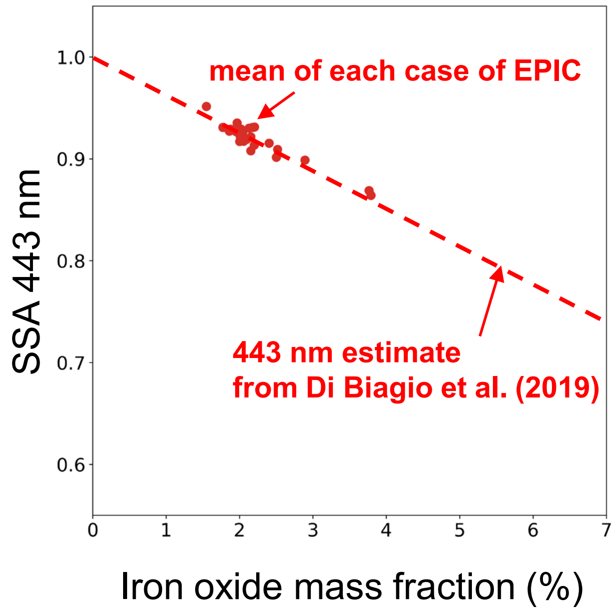

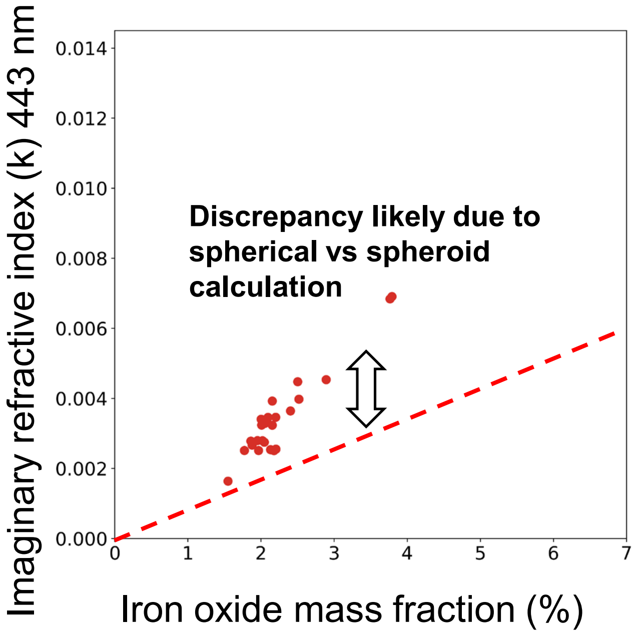

Di Biagio et al. (2019)

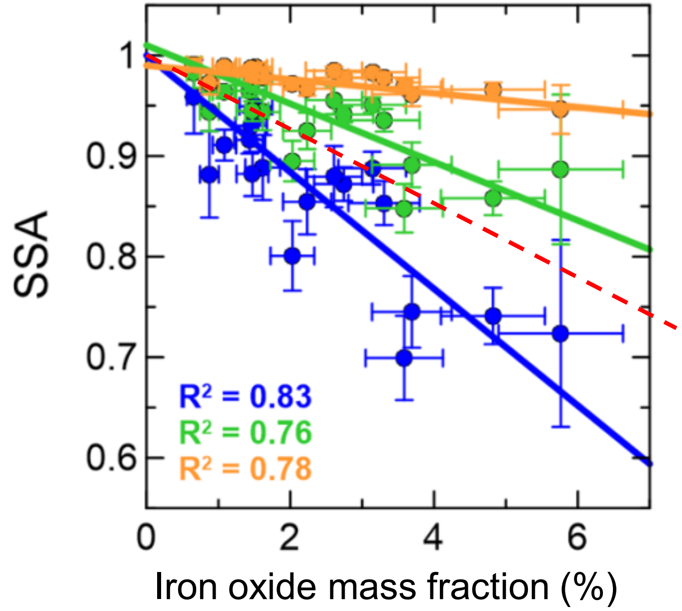

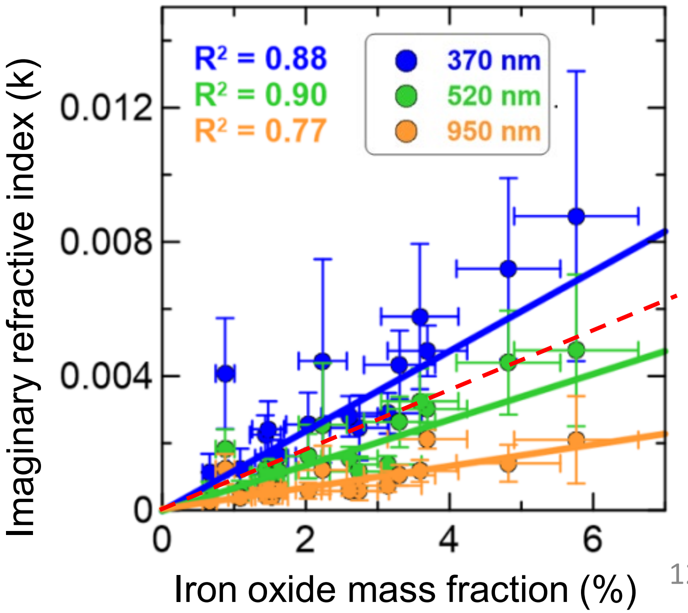

Moosmüller et al. (2012); Di Biagio et al. (2019)

- found the relationships between k, SSA, and the iron oxide or elemental iron content in dust create an opp ortunity to establish predictive rules to estimate the spectrally resolved SW absorption of dust based on composition.

Di Biagio et al. (2019)

- Refractive index are estimated by "Mie" calculation : from optical, size data
- SSA are estimated directly from "scattering and abs orption" coefficient.
- SSA(or k) linearly decrease(or increase)

Comparison with Di Biagio et al. (2019)

- **Shaded area : EPIC retrieved**
  - Monthly composite of Hematite / Goethite (5^{th}, median, 95^{th})
  - With pixels of AOD>1.0 used only
  - ± 1 degree box pixels collected (Monthly)
  - 01/01/2018 – 12/31/2018 (1 year)
  - **Soil content + affected by transport due to different source regions**

- **Dashed line : Di Biagio et al. (2019)**
  - ± 10% uncertainty
  - Simulation chamber study (with X-ray absorption near edge structure (XANES) method), from soil samples and sediments collected from each desert area
  - Refer to the bulk composition of pure dust aerosol in dry condition with a size range of 2-6day transport.
  - **Soil content only**

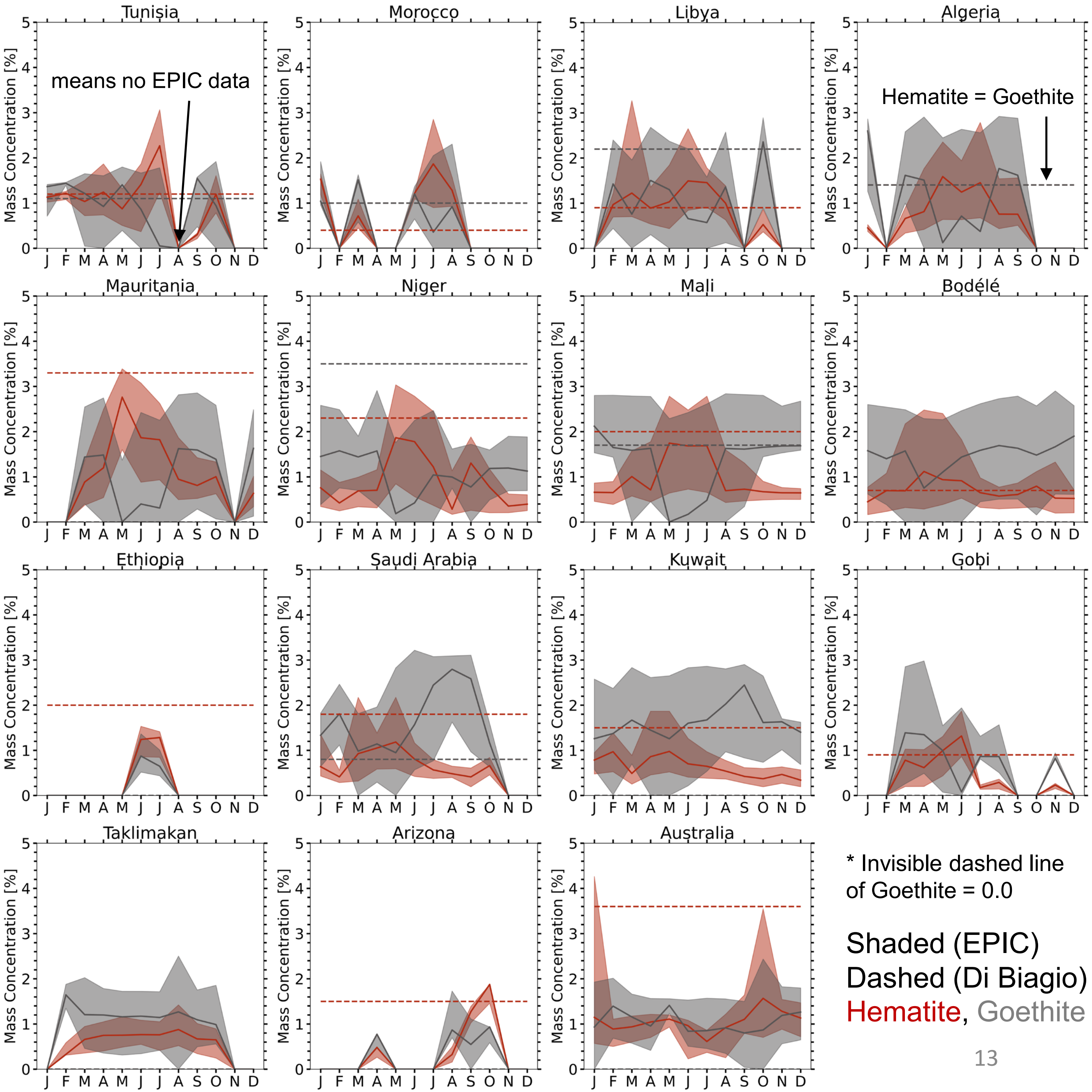

* Invisible dashed line of Goethite = 0.0

Shaded (EPIC)
Dashed (Di Biagio)
Hematite, Goethite

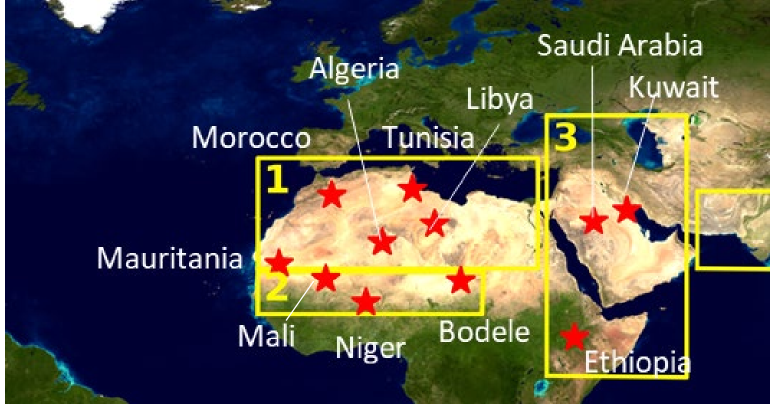

- Sahara, Sahel, Middle East → large variability
- Sahel line (~20°N) hematite tendency
  - EPIC: Mauritania > Niger > Mali > Bodélé
  - Di Biagio: (3.3%) > (2.3%) > (2.0%) > (0.7%)
- Niger (Lafon et al., 2004)
  - Harmattan (11-3): 2.8% iron oxide → agrees
  - Local erosion (5-7): 5.0% (±0.4) iron oxide
    → Possibly due to rain, MAIAC did not catch
- Bodélé:
  - EPIC: consistently low hematite (<1.4%)
  - Di Biagio: 0.7% hematite
- Saudi Arabia, Kuwait:
  - Shamal season (6-9): northwesterly wind
    → hematite, goethite reversed
- Gobi, Taklimakan:
  - Hm/Gt ratio ~ 0.55 observed (Shen et al., 2006)
- Arizona, Australia: may contain smoke cases, but case study agreed with dashed line range.

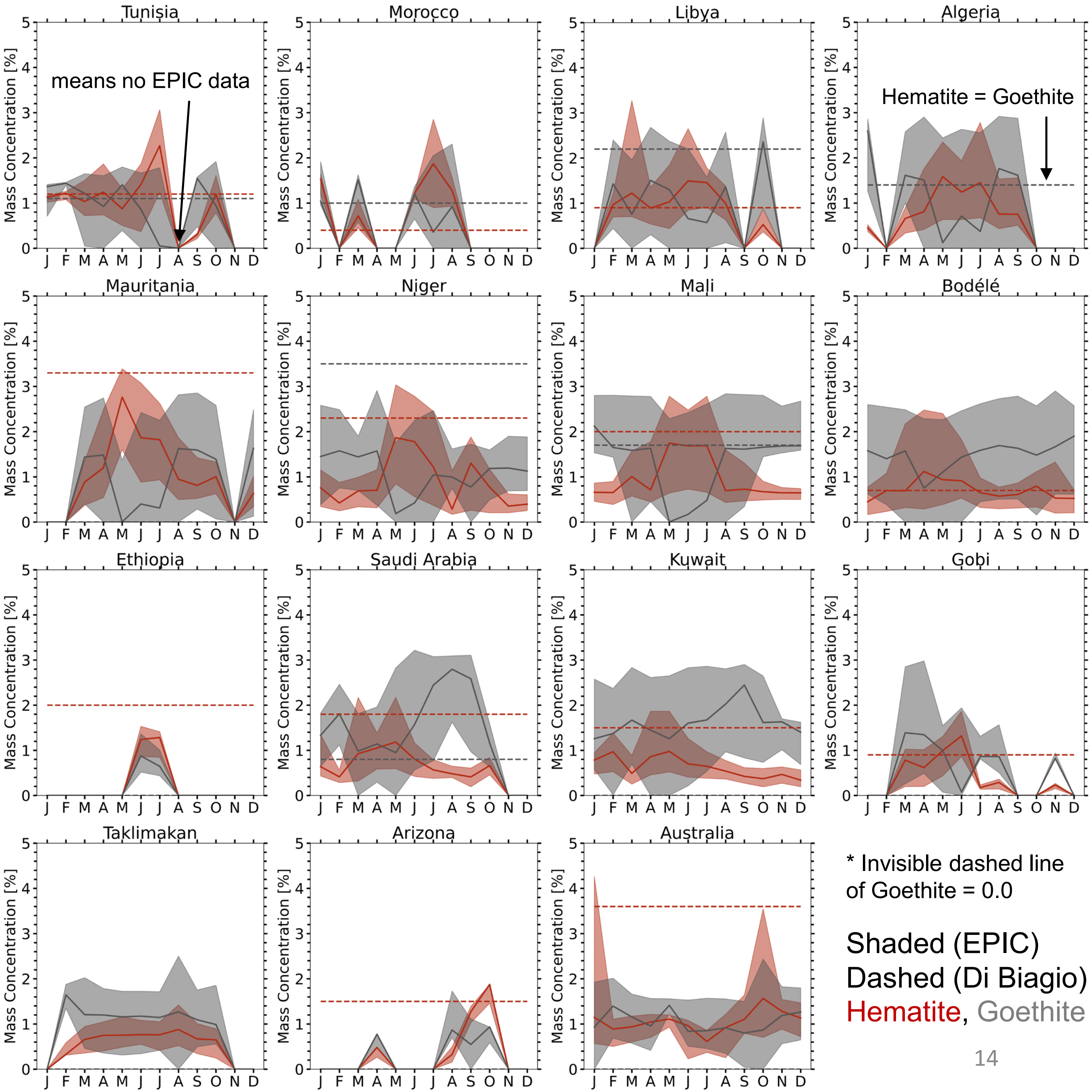

Hematite refractive indices exhibit a large range in the literature

13 different hematite refractive indices

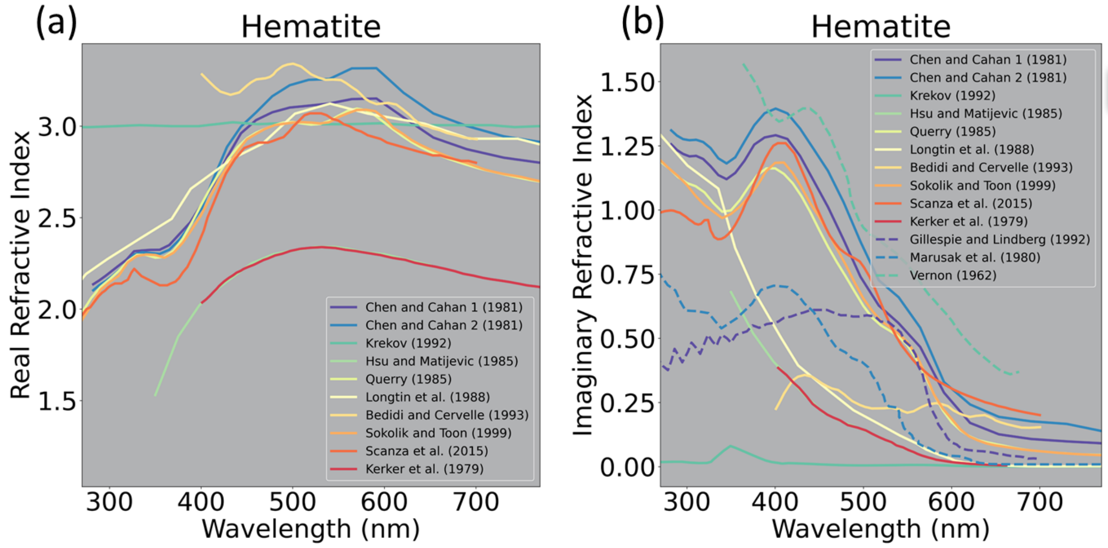

After exclude: Most suitable hematite refractive index

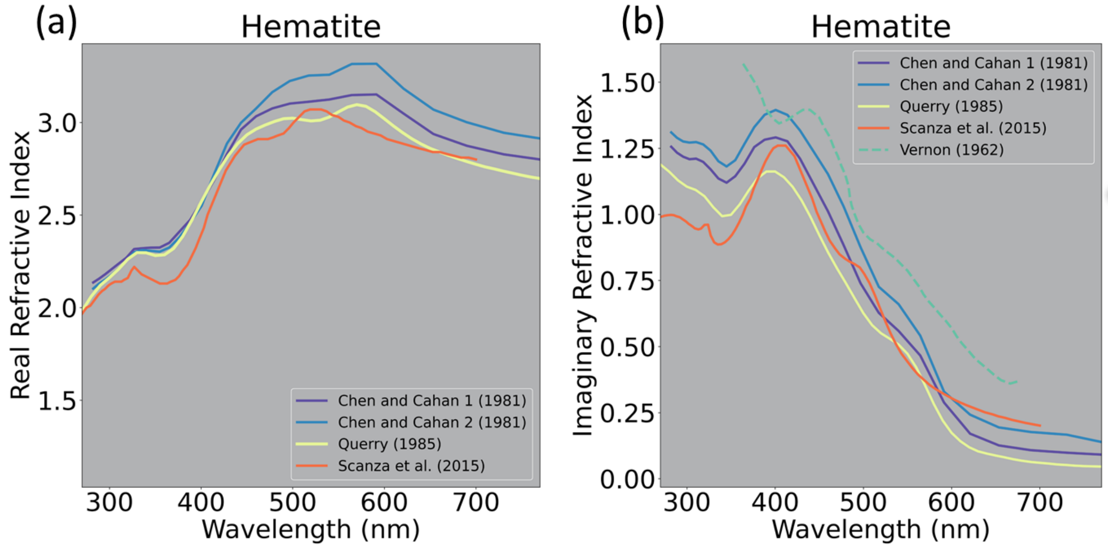

Same dust event but with
13 different models of hematite refractive index

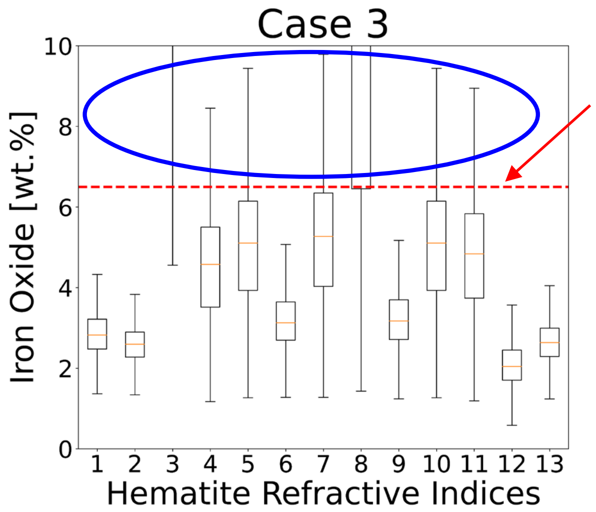

maximum expected iron-oxide content (6.5 wt.%) based on *in situ* measurements

1. Chen and Cahan 1 (1981)
2. Chen and Cahan 2 (1981)
3. ~~Krekov (1992)~~
4. ~~Gillespig and Lindberg (1992)~~
5. ~~Hsu and Matijevic (1985)~~
6. Querry (1985)
7. ~~Longtin (1988)~~
8. ~~Bedidi and Cerville (1993)~~
9. Sokolik and Toon (1999)
10. ~~Kerker (1979)~~
11. ~~Marusak (1980)~~
12. Vernon (1962)
13. Scanza (2015) **– this study**

→ 3,4,5,7,8,10,11 are not viable for our approach

Climatology of iron oxides species

- Pixels of AOD>1.0 used only
- 01/01/2018 – 12/31/2018 (1 year)

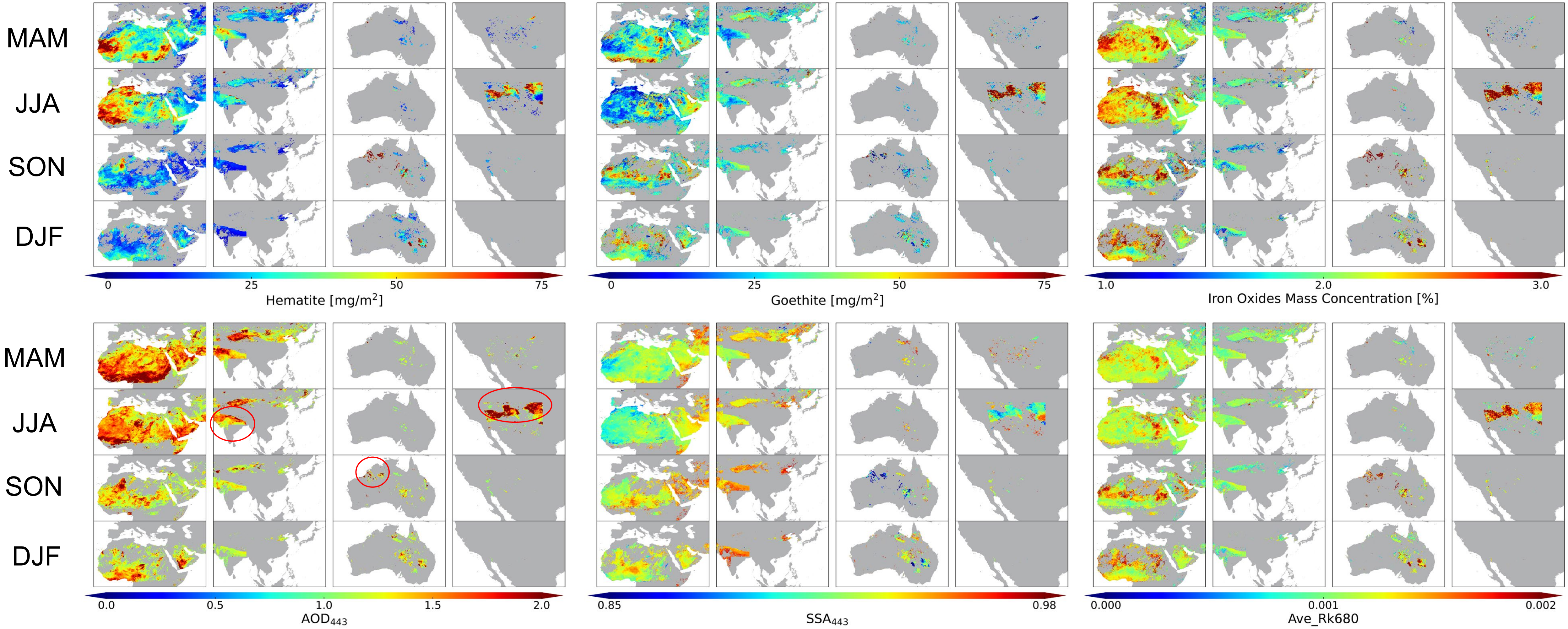

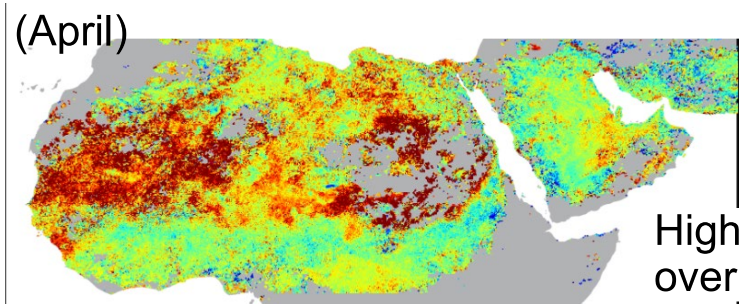

High Iron oxide over Sahel

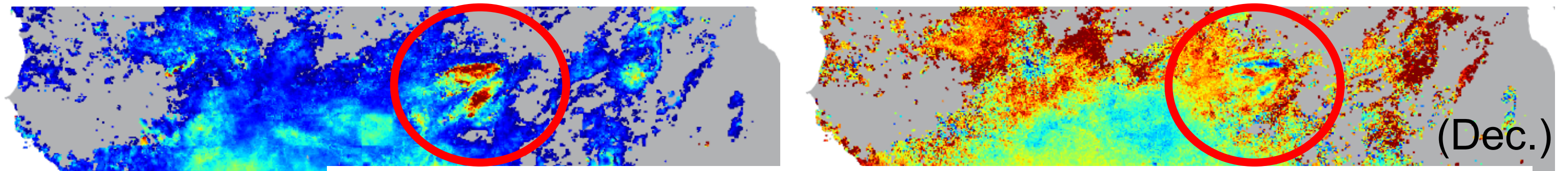

High AOD > 2.0 (left) with low iron oxides content ~1% (right) throughout the year captured over Bodélé.

From EPIC AOD to composition mass concentration <u>for smoke</u>

- Smoke aerosol = composed of a host of sulfate-nitrate-ammonium (SNA) and two absorbing inclusions BC and BrC
- Step 1: calculate total (fine + coarse) volume concentration of smoke (440 nm)
  - $\tau^a = \tau_f^a + \tau_c^a = C_{Vf}h_f + C_{Vc}h_c$
    $= C_{Vf}\left(h_f + h_c\left(C_{Vc}/C_{Vf}\right)\right) = C_{Vf}\ (7.6461 +\ 0.7235\ * 1/2.5) = 7.9355 * C_{Vf}$
  - $C_V = C_{Vf} + C_{Vc} = C_{Vf}\left(1 + C_{Vc}/C_{Vf}\right) = \frac{\tau^a}{7.9355}(1 + 1/2.5) = 0.1764\ * \tau^a$
  - Unit of C_V: μm³/μm²

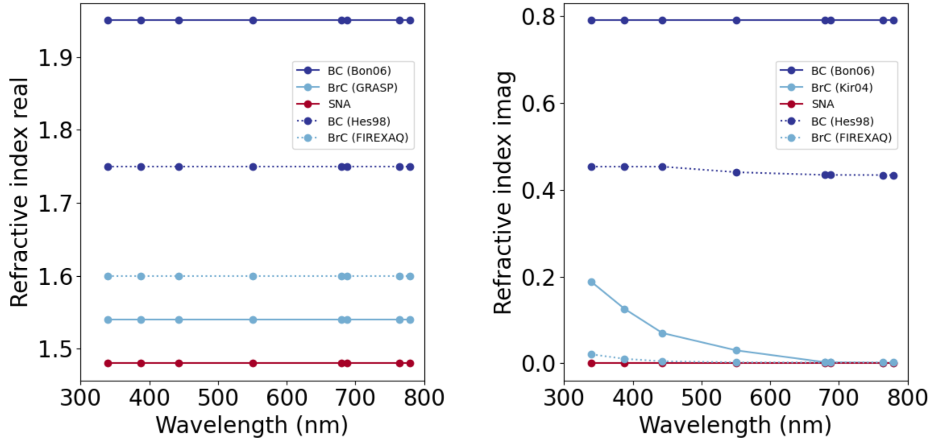

- Step 2, Step 3 same as dust with ρ_{BC}= 1.8 g/cm³, ρ_{BrC}= 1.2 g/cm³

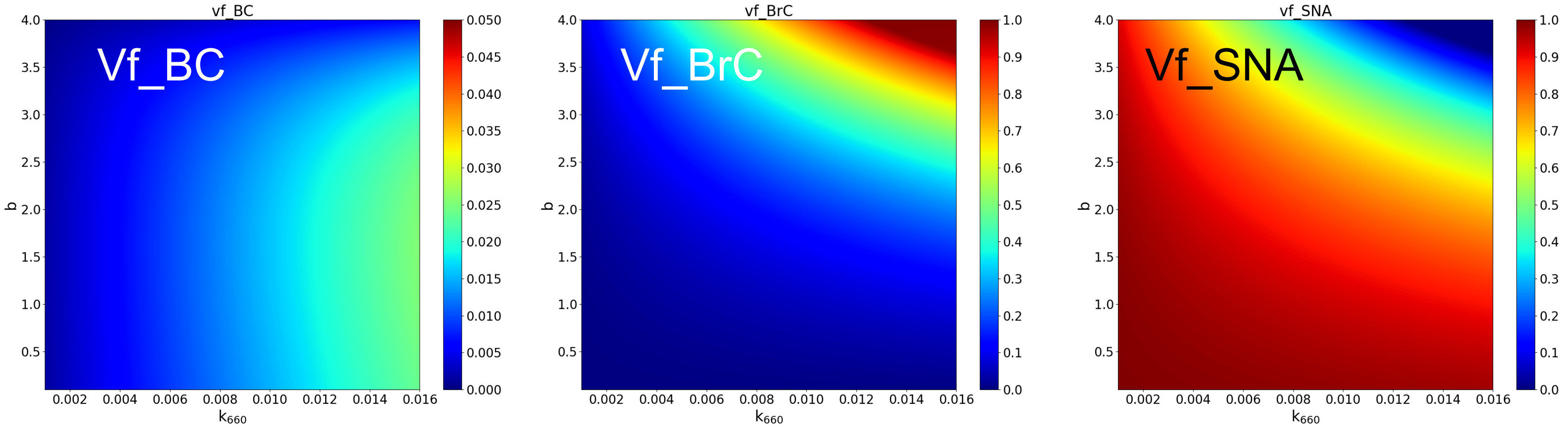

Volume fraction range of (a) BC, (b) BrC, and (c) SNA according to k_{680} and b

Contrasting Regional Aerosol Properties – BC and BrC

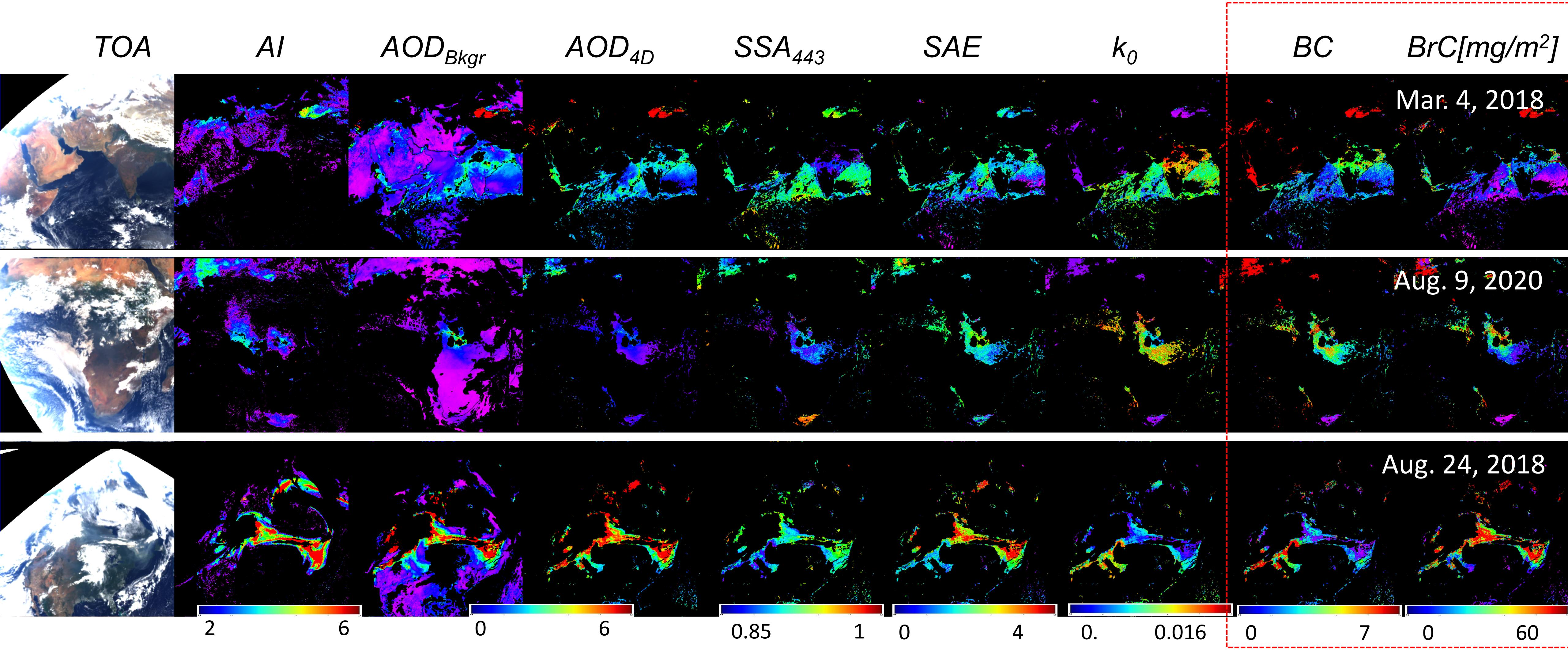

1. USA: Forest wildfires: moderate abs., SSA~0.9-0.94, **high BrC** (SAE), **low-moderate BC** (k_0), ALH can be very high.
2. India, South Africa biomass burning: bush- and grasslands, agriculture crop residue etc. (low energy fast burning): high absorption, SSA~0.85-0.88, **low-moderate BrC** (SAE), **high BC** (k_0), ALH is low (<1-1.5km).

Conclusion

- Information of iron oxides content and their apportionment between hematite (α-Fe_2O_3) and goethite (α-FeOOH) species are key determinants of quantifying shortwave dust DRE estimate in Earth system model. Here, contents of hematite (α-Fe2O3) / goethite (α-FeOOH) column are inferred from single-viewing satellite EPIC at ultraviolet–visible (UV-Vis) channels globally over major global dust source regions using MG EMA internal mixing rule.

- Retrieved iron oxides enveloped the overall range of Di Biagio et al. (2019) soil measurement data of iron oxides 0.7-5.8% and were in line with the previous published results generally. The ratio between hematite and goethite over Sahel was different between Harmattan and summer season, thereby implying considerable seasonal and temporal variation attributed to different source regions. Likewise, the ratio between hematite and goethite over the Middle East tends to change before and after shamal season. Globally, the Sahel region represented higher iron oxides than Sahara especially in April. Lower iron oxide content over Bodélé due to its diatomic sediments with high AOD were clearly observed throughout the year.

- Combining the VIIRS fire detection and the EPIC MAIAC smoke aerosol products, including BC and BrC, confirmed that freshly emitted smoke aerosols from North America wildfires exhibited high fractions of BC and BrC near sources and the absorption decreased as transported to surroundings.

- The algorithm can be applied for other nadir-viewing instruments having UV-Vis channels, thereby will be beneficial for dust/smoke DRE related climate change (e.g., input for climate models) / air quality (e.g., epidemiology) study.